Step-Edge-Induced Anisotropic Chiral Spin Coupling in Ultrathin Magnetic Films

A. Schlenhoff,[*] S. Krause, and R. Wiesendanger
Department of Physics, University of Hamburg, Jungiusstrasse 11A, 20355 Hamburg, Germany

(Received 3 December 2018; published 17 July 2019)

Step edges represent a local break of lateral symmetry in ultrathin magnetic films. In our experiments, we investigate the spin coupling across atomic step edges on Fe/$W(110)$ by means of spin-polarized scanning tunneling microscopy and spectroscopy. Local modifications of the spin texture toward step edges separating double from single layer areas are observed, and selection rules indicate a chiral spin coupling that significantly changes with the propagation along the $[1\bar{1}0]$ or the [001] crystallographic direction. The findings are explained via anisotropic Dzyaloshinskii-Moriya interactions arising from the broken lateral symmetry at atomic step edges.

DOI: 10.1103/PhysRevLett.123.037201

The Dzyaloshinskii-Moriya interaction (DMI) [1,2] in magnetic systems lacking inversion symmetry and exhibiting strong spin-orbit coupling has raised great interest both theoretically and experimentally. It prefers a 90° rotation of neighboring atomic spins with a fixed rotational sense. In competition with exchange and magnetocrystalline anisotropy, DMI can lead to complex noncollinear spin structures in thin films, like chiral domain walls, spin spirals, and magnetic skyrmions [3–6]. In most thin film systems that have been studied up to now, the DMI is induced by the lack of inversion symmetry at the planar interface between a heavy-element substrate and a heteroepitaxial thin film. The energy gained or lost due to a DMI-induced chiral spin coupling between two spins is described by

$$E_{\mathrm{DMI}} = \vec{D} \cdot (\hat{s}_1 \times \hat{s}_2). \tag{1}$$

Here, the direction and orientation of the characteristic DMI vector $\vec{D}$ defines the preferred chiral coupling between the local spins with their unit vectors pointing along $\hat{s}_1$ and $\hat{s}_2$, respectively. Conventionally, both spins are considered to be part of a system that exhibits a high degree of inversion symmetry parallel to the surface or interface plane. However, atomic step edges on surfaces or interfaces of ultrathin magnetic films locally break this lateral inversion symmetry. The question remained open whether such a local lack of symmetry in combination with a substrate providing strong spin-orbit coupling gives rise to DMI, resulting in a chiral spin coupling across the step edges.

As we show in our experiments, atomic step edges induce a chiral spin coupling, with outreaching consequences on the local spin texture in the film. For ultrathin magnetic films with the easy axis of magnetization changing direction for different coverages, a spin rotation is enforced at step edges. Such a model system of alternating magnetic easy axes is realized by preparing atomic layers of Fe/$W(110)$, with single atomic step edges separating Fe double layer (DL) from monolayer (ML) areas. It has been investigated intensively due to its interesting magnetic properties. Whereas the ML has a ferromagnetic order with the easy axis of magnetization pointing along the $[1\bar{1}0]$ in-plane direction [7,8], the DL exhibits an easy axis of magnetization perpendicular to the film plane due to strong out-of-plane magnetic anisotropy [3,9]. The DMI arising from the strong spin-orbit coupling and the symmetry breaking at the interface between the ultrathin Fe film and the W substrate causes the Néel-type domain walls of the DL having a unique rotational sense and propagating along the [001] direction [10–13]. Here, we show by spin-polarized scanning tunneling microscopy (SP-STM) experiments that atomic step edges in an ultrathin Fe/$W(110)$ film additionally induce DMIs arising from the lack of lateral symmetry, resulting in a highly anisotropic chiral coupling of DL spins to the ML.

The experiments were performed under ultrahigh vacuum conditions with a pressure below 1×10^{-8} Pa using a homebuilt spin-polarized scanning tunneling microscope at a temperature of 41 K and in absence of any external magnetic field. Within our experimental setup, the entire microscope including the magnetic tip is cooled to maximize the thermal stability. The $W(110)$ substrate was cleaned by annealing in oxygen as described in Ref. [14]. Nominally 1.5 atomic layers of Fe were deposited by molecular beam epitaxy and subsequent annealing at 550 K for four minutes. Simultaneously to constant current topography images at closed feedback loop (set point $I = 2$ nA), a small ac modulation voltage ($U_{\mathrm{mod}} = 40$ mV, $f = 4.333$ kHz) was added to the applied bias voltage U in order to record the spatially resolved differential tunneling conductance $dI/dU(\vec{r})$ between tip and sample by lock-in technique. Since $dI/dU(\vec{r})$ scales with the cosine of the enclosed angle between the magnetic moments of the tip and the sample at the location $\vec{r}$, the resulting dI/dU maps correlate with the magnetization structure of the sample [15]. For the SP-STM experiments, antiferromagnetic bulk Cr tips were used to avoid undesired dipolar coupling with the sample. As these tips generally exhibit a canted spin polarization, they allow for a spin sensitivity on both the ML as well as on the DL [16].

Figure 1(a) shows a topography overview of the prepared Fe/$W(110)$ sample surface. Regions of pseudomorphic ML and DL coverages coexist. As has been observed before, the ML forms a wetting layer on the $W(110)$ substrate, and the strong lattice mismatch between W and Fe results in the formation of dislocation lines in the DL, propagating along the [001] direction [17]. On the extended $W(110)$ terraces, step edges between ML and DL coverages are formed, preferentially aligning along the [001] direction. The corresponding magnetic SP-STM map is shown in Fig. 1(b). Two different dI/dU signal levels are

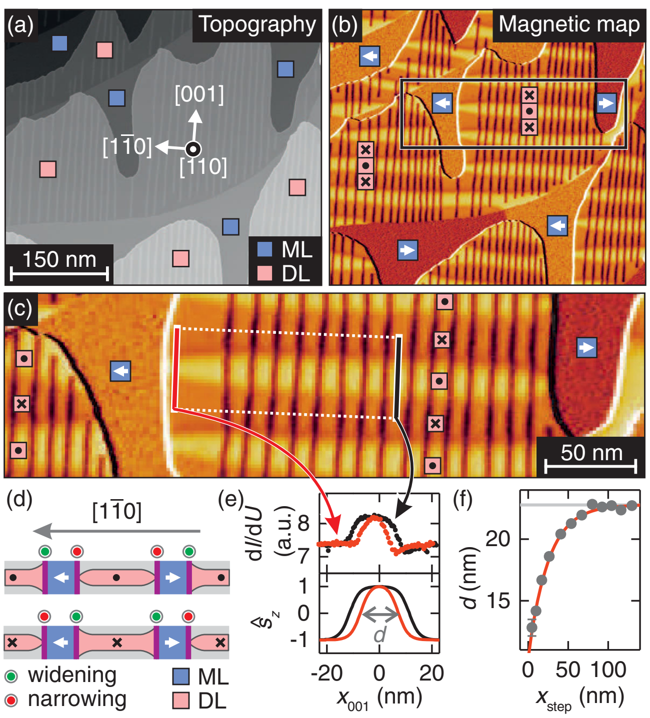

FIG. 1. (a) STM topography image of the Fe/$W(110)$ sample surface. ML and DL areas are visible. (b) Simultaneously recorded magnetic SP-STM map. The magnetization structure on the sample is indicated by the symbols. (c) Closer view of the area marked in (b). A deformation of the DL domain structure toward the step edges is observed. (d) Experimentally observed widening or narrowing of DL domains coupled to the ML along the $[1\bar{1}0]$ direction across atomic step edges. (e) Top: Magnetic line profile along the [001] direction, taken close to (red) and far away from (black) a step edge, as indicated by the lines in (c). Bottom: Line profiles of the out-of-plane component $\hat{s}_z$ of the spin unit vector as determined from fitting the data, yielding the domain wall pair distance d. (f) Results for d as function of step edge distance x_{step}. ($I = 2$ nA, $U = 100$ mV.)

observed on the ML, indicating its ferromagnetic domain structure with uniaxial magnetic anisotropy. In the DL the dislocation lines appear as dark lines. Additionally, a periodic pattern of bright and dark domains is visible that evolves along the [001] direction. Toward the step edges, this pattern is significantly deformed: Whereas the overall periodicity of the domain structure remains constant, a strong asymmetry of domains with spins pointing out of and into the surface plane develops. The ferromagnetic ML is apparently not affected by the presence of step edges. A closer view of the magnetic map is shown in Fig. 1(c), spanning four step edges between ML and DL areas on an extended $W(110)$ terrace. At the step edges, DL domains with spins perpendicular to the film plane increase or decrease in size, depending on the orientation of the spins in the adjacent ML. This selective widening or narrowing of the DL domains toward the step edges is found be to characteristic for the system [18]. It indicates a chiral Néel-type spin coupling between the ML and the DL when propagating along the $[1\bar{1}0]$ direction and crossing Fe step edges on an atomically flat $W(110)$ terrace. It competes with the formation of the domain pattern in the DL along the [001] direction and therefor results in the widening (narrowing) of the DL domains with the preferred (avoided) spin configuration at the step edges, as depicted in Fig. 1(d). We attribute the chiral spin coupling between DL and ML spins to the local DMI induced by the symmetry break at the step edges in the magnetic film, resulting in the deformation of the DL spin texture. The corresponding DMI vector $\vec{D}_{1\bar{1}0}$ aligns parallel to the step edge, i.e., along the [001] direction. The magnitude of $\vec{D}_{1\bar{1}0}$ is estimated by analyzing cross sections of the spin texture as a function of step edge distance. In the top panel of Fig. 1(e), two exemplary magnetic line profiles spanning one period on the DL are shown, as recorded in close vicinity to and far away from a step edge. The deformation of the spin structure toward the step edge is clearly visible. Despite of their Néel-type character, a 180° Bloch wall model was shown to apply for the analysis of the DL domain walls in terms of position and width [3]. We fitted our data with the model, yielding the local spin phases and the domain wall widths w as a function of step edge distance. In the lower panel of Fig. 1(e), the out-of-plane component $\hat{s}_z$ of the local spins is shown, as derived from the fitting. In contrast to $w = (7.6 \pm 0.2)$ nm, which is found to be constant, the domain width d, defined by the distance between the two domain walls, drastically changes toward the step edge. The evolution of d with increasing step edge distance is shown in Fig. 1(f). It is generated from fitting numerous profiles taken within the dotted rectangle marked in Fig. 1(c). Obviously, the deformation reaches far into the DL: Only when being more than about 80 nm away from the step edge the domain walls exhibit a constant distance of (22.8 ± 0.1) nm. Calculation of the total energy per period and integration over $x_{1\bar{1}0}$ yields the total deformation energy which is compensated by the DMI at the step edge, resulting in $D_{1\bar{1}0} \approx 1.5\ \mathrm{mJ/m^2}$ [18]. The DMI causing the sequence of Néel-type domain walls with unique rotational sense in the extended DL film is $6.4\ \mathrm{mJ/m^2}$ [13]. This DMI of the extended film locally competes with the edge-induced DMI, resulting in a considerable deformation of the periodic spin texture in the DL.

Figure 2(a) shows a magnetic map recorded on the same sample with the same tip, but on a different area. Here, the terraces on the $W(110)$ surface are much smaller, resulting in the step-flow growth of narrow DL stripes that are terminated by domains with the magnetization pointing out of the film plane. In this area the spin coupling along the [001] direction across atomic step edges between the DL and the ML is investigated. Representations of all four possible magnetic configurations (top view and propagating along the [001] direction: $\otimes\uparrow; \otimes\downarrow; \odot\uparrow; \odot\downarrow$) at the step edges between DL and ML coverages are found on the sample surface, as shown in Fig. 2(a). Corresponding magnetic line profiles along the [001] direction across step edges are shown in the left column of Fig. 2(b). Either a gradual spin rotation by 90° toward the step edges or a fixed out-of-plane spin orientation up to the step edge is observed on the DL, indicating a selection rule for the spin coupling across the step edges. The detailed spin structure around the step edges can be constructed by fitting the DL data with a 180° domain wall model [3]. In the right column of Fig. 2(b) the relative change of spin phase $\Delta\phi$ with respect to the easy magnetic axis of the DL is shown for each configuration. For a clockwise spin rotation from the DL to the ML ($\Delta\phi > 0$, corresponding to $\otimes\uparrow$ and $\odot\downarrow$), a 90° Bloch wall is realized within the DL, whereas no spin rotation is observed in the DL for the counterclockwise rotation with $\Delta\phi < 0$ ($\otimes\downarrow$ and $\odot\uparrow$). This selection rule applies when crossing a step edge along the [001] direction, irrespectively of its orientation along the $[1\bar{1}1]$ or $[\bar{1}11]$ direction. This experimental finding indicates a very strong step-edge-induced spin coupling along [001].

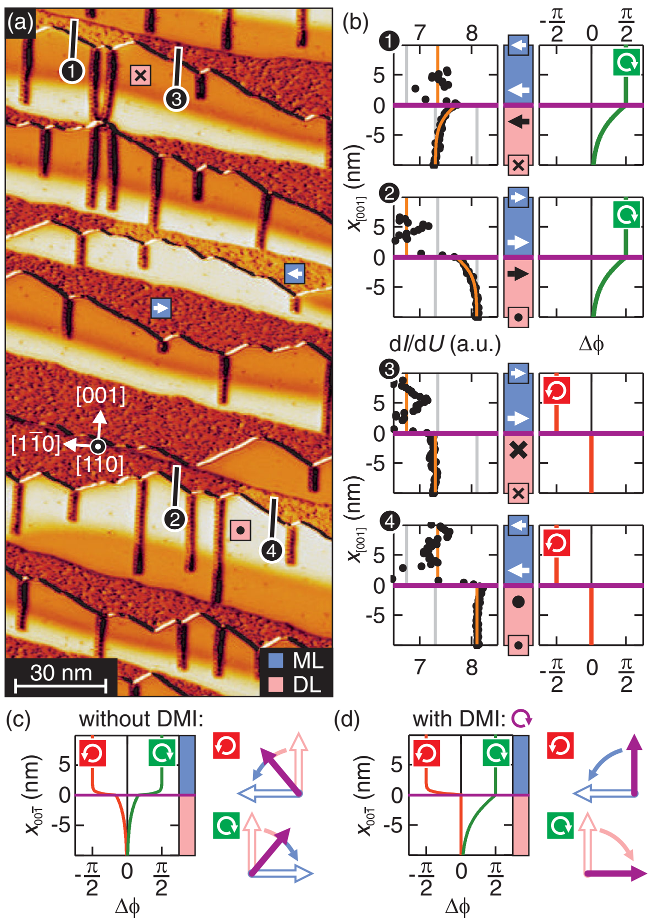

FIG. 2. (a) Magnetic SP-STM map taken with the same probe tip on the same sample, but on a different area. ML and DL areas and the spin structure are indicated by symbols ($I = 2$ nA, $U = 100$ mV). (b) Left: Line profiles taken along the [001] direction across step edges, as indicated in (a). Orange: Average spin signal on the ML and DL for the respective spin configuration. Center: Spin configuration at the step edge, as determined from the experiment. Right: Change of spin phase $\Delta\phi$ with respect to the DL domain, when crossing the step edge. (c) $\Delta\phi$, as theoretically determined by a spin coupling model in absence of DMI, for clockwise and counterclockwise rotation. (d) Same situation like in (c), but with considerable DMI. Here, spin rotation is fully realized within either the DL or the ML, thereby lifting the rotational degeneracy.

It is known from previous studies that DL islands with diameters less than the exchange length ($l_{\mathrm{DL}} = 3.3$ nm) exhibit a ferromagnetic in-plane magnetization, driven by the local exchange coupling of the DL to the ML [9,19,20]. As has been shown in a theoretical study based on a micromagnetic model, it is this exchange coupling that locally deforms the otherwise ferromagnetic spin texture at the step edges separating extended DL areas from the ML [21]. In absence of DMI, a gradual spin rotation $\Delta\phi$ by 90° extends from the DL into the ML, as shown in Fig. 2(c). In the equilibrium state, the spin tilt at the step edge is defined by the vanishing exchange torque between DL and ML spins, being degenerate for clockwise and counterclockwise spin rotation. Our experiments indicate a lifting of this degeneracy, with a rotation of the DL spins by 90° for $\Delta\phi > 0$, whereas it is suppressed for $\Delta\phi < 0$. Consequently, a chiral coupling induced by DMI has to be considered. It generates a local spin torque at the step edge that adds to the exchange torque and thereby modifies the equilibrium spin texture. We extended the spin coupling model by introducing DMI and solved it for the equilibrium state [18]. In accordance with our experimental findings, we find that the spin rotation is completely localized either in the DL or the ML area for sufficiently large DMI, depending on the sense of the spin rotation across the step edge. In Fig. 2(d), the respective model spin configurations

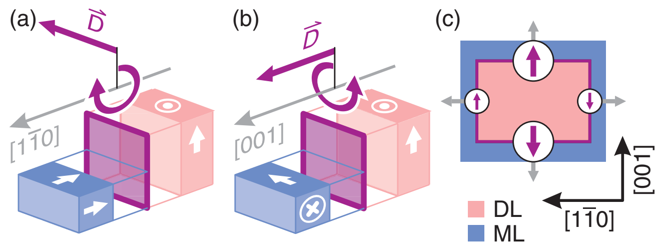

FIG. 3. Chiral spin coupling between DL and ML areas of Fe/$W(110)$ across atomic step edges and respective DMI vector $\vec{D}$ for a propagation along the (a) $[1\bar{1}0]$ and (b) [001] direction. (c) Sketch of the DMI vectors for crossing step edges from the DL to the ML.

across a DL-ML step edge are shown for both rotational senses. The exchange length in the ML is very small ($l_{\mathrm{ML}} \leq 0.3$ nm) [8]. Consequently, the spin rotation within the ML, as indicated by the model for $\Delta\phi < 0$ cannot be observed in the SP-STM images. As the spin coupling across the step edges is Bloch-like, the DMI vector $\vec{D}_{001}$ for the spin coupling along the [001] direction is pointing parallel to this direction. From our spin coupling model, the critical magnitudes of the DMI D_{001} are calculated, once for $\Delta\phi < 0$ and $\Delta\phi > 0$, based on the DL and ML material parameters [18]. We constructed the detailed spin textures around the step edges from the model, and comparison with the experimental data results in $D_{001} \approx 5.5$ mJ/m^2 [18]. This value is significantly larger than the step-edge-induced DMI along the $[1\bar{1}0]$ direction, thereby dominating over $D_{1\bar{1}0}$.

The experimental findings for the DMI vectors are summarized in Fig. 3. When crossing a step edge along the $[1\bar{1}0]$ direction, the corresponding DMI vector $\vec{D}_{1\bar{1}0}$ is perpendicular to the propagation direction, indicating chiral Néel-type spin coupling, as shown in Fig. 3(a). In contrast, the DMI vector $\vec{D}_{001}$ is parallel to the propagation direction when crossing a step edge along the [001] direction, resulting in a chiral Bloch-type spin coupling, as shown in Fig. 3(b). The experimental findings for the DMI in the DL-ML step edges are schematically summarized in Fig. 3(c). Note that the magnitude and the direction of the DMI vectors are highly direction dependent, indicating a considerable anisotropy of the DMI. For extended ML and DL Fe/$W(110)$ films a sign change in the DMI along different high-symmetry directions has been predicted theoretically [22–26], but has not yet been experimentally proven. Here, we show experimental evidence for an anisotropic DMI, arising from atomic step edges with different orientations on a bcc(110) surface. Anisotropic DMI is predicted to generate multichiral spin textures, like antiskyrmions [26]. Based on our findings we expect atomic-scale adlayer dots on anisotropic magnetic surfaces with high spin-orbit coupling to be potential model systems for the investigation of these multichiral spin structures.

In summary, our study shows that atomic step edges in ultrathin magnetic films drastically modify the local spin texture. The SP-STM experiments reveal an anisotropic chiral spin coupling across Fe/$W(110)$ DL-ML step edges, driven by DMI arising from the local lack of lateral symmetry. Our findings indicate that surface roughness and interface quality on the atomic scale is of high relevance for spin manipulation and transmission in terms of tailored magnetic coupling for future spintronic applications.

Financial support from the DFG via Grants No. SCHL 2096/1-1 and No. SPP 2137 Skyrmionics is gratefully acknowledged.

*aschlenh@physnet.uni-hamburg.de

[1] I. E. Dzyaloshinskii, Sov. Phys. JETP **5**, 1259 (1957).
[2] T. Moriya, Phys. Rev. **120**, 91 (1960).
[3] A. Kubetzka, O. Pietzsch, M. Bode, and R. Wiesendanger, Phys. Rev. B **67**, 020401(R) (2003).
[4] K. von Bergmann, S. Heinze, M. Bode, G. Bihlmayer, S. Blügel, and R. Wiesendanger, New J. Phys. **9**, 396 (2007).
[5] S. Heinze, K. von Bergmann, M. Menzel, J. Brede, A. Kubetzka, R. Wiesendanger, G. Bihlmayer, and S. Blügel, Nat. Phys. **7**, 713 (2011).
[6] N. Romming, C. Hanneken, M. Menzel, J. E. Bickel, B. Wolter, K. von Bergmann, A. Kubetzka, and R. Wiesendanger, Science **341**, 636 (2013).
[7] H. J. Elmers, J. Hauschild, and U. Gradmann, Phys. Rev. B **54**, 15224 (1996).
[8] M. Pratzer, H. J. Elmers, M. Bode, O. Pietzsch, A. Kubetzka, and R. Wiesendanger, Phys. Rev. Lett. **87**, 127201 (2001).
[9] H. J. Elmers, J. Hauschild, and U. Gradmann, Phys. Rev. B **59**, 3688 (1999).
[10] A. Kubetzka, M. Bode, O. Pietzsch, and R. Wiesendanger, Phys. Rev. Lett. **88**, 057201 (2002).
[11] E. Y. Vedmedenko, L. Udvardi, P. Weinberger, and R. Wiesendanger, Phys. Rev. B **75**, 104431 (2007).
[12] S. Meckler, N. Mikuszeit, A. Preßler, E. Y. Vedmedenko, O. Pietzsch, and R. Wiesendanger, Phys. Rev. Lett. **103**, 157201 (2009).
[13] S. Meckler, O. Pietzsch, N. Mikuszeit, and R. Wiesendanger, Phys. Rev. B **85**, 024420 (2012).
[14] M. Bode, S. Krause, L. Berbil-Bautista, S. Heinze, and R. Wiesendanger, Surf. Sci. **601**, 3308 (2007).
[15] R. Wiesendanger, Rev. Mod. Phys. **81**, 1495 (2009).
[16] A. Schlenhoff, S. Krause, G. Herzog, and R. Wiesendanger, Appl. Phys. Lett. **97**, 083104 (2010).
[17] H. Bethge, D. Heuer, C. Jensen, K. Resöft, and U. Köhler, Surf. Sci. **331–333**, 878 (1995).
[18] See Supplemental Material at http://link.aps.org/supplemental/10.1103/PhysRevLett.123.037201 for additional data and model details.
[19] N. Weber, K. Wagner, H. J. Elmers, J. Hauschild, and U. Gradmann, Phys. Rev. B **55**, 14121 (1997).
[20] A. Kubetzka, O. Pietzsch, M. Bode, and R. Wiesendanger, Phys. Rev. B **63**, 140407(R) (2001).

[21] H. Elmers, J. Magn. Magn. Mater. **185**, 274 (1998).
[22] M. Heide, Ph.D. thesis, RWTH Aachen, 2006.
[23] M. Heide, G. Bihlmayer, and S. Blügel, Phys. Rev. B **78**, 140403(R) (2008).
[24] B. Zimmermann, M. Heide, G. Bihlmayer, and S. Blügel, Phys. Rev. B **90**, 115427 (2014).
[25] L. Rózsa, L. Udvardi, L. Szunyogh, and I. A. Szabó, Phys. Rev. B **91**, 144424 (2015).
[26] M. Hoffmann, B. Zimmermann, G. P. Müller, D. Schürhoff, N. S. Kiselev, C. Melcher, and S. Bügel, Nat. Commun. **8**, 308 (2017).